社団法人　電子情報通信学会
THE INSTITUTE OF ELECTRONICS,
INFORMATION AND COMMUNICATION ENGINEERS

信学技報
TECHNICAL REPORT OF IEICE.

屋内伝搬実験に基づくRF適応アンテナの特性評価

田中　宏哉† 　クリアンサック シワソンディワット† 　高田　潤一† 　本田　敦††
ソルワル ホセイン††
井田　一郎†† 　大石　泰之††

† 東京工業大学大学院 理工学研究科 国際開発工学専攻　〒 152–8550 東京都目黒区大岡山 2–12–1–S6–4
†† 富士通株式会社　〒 239–0847 神奈川県横須賀市光の丘 5–5
E-mail: †{tanaka,joe,takada}@ap.ide.titech.ac.jp
††{ahonda@labs.fujitsu.com, s.hossain@jp.fujitsu.com, ida.ichirou@jp.fujitsu.com, yasu@labs.fujitsu.com}

あらまし　近年，RF 帯でアンテナの適応制御を行い通信の性能向上を図るシステム (RF 適応アンテナ) による MIMO 伝送の高能率化に関する報告がなされている．代表例として，(1)RF スイッチを適応制御することによりアンテナ選択を行うアンテナ選択型，(2) エスパアンテナによるビームステアリング型適応アンテナが挙げられる．これらの RF 適応アンテナは動作原理は違うものの，通信システムの性能向上を図るという面で同じコンセプトを有していると言える．本報告では，屋内伝搬実験で得られた見通し内環境および見通し外環境での伝搬モデルを基に，上記の異なる RF 適応アンテナの性能比較を行う．上記見通し内及び見通し外環境下で複数のアンテナ方向を向けた場合における平均伝送容量を解析した結果，エスパアンテナがスイッチを用いたアンテナ選択よりもそれぞれ 1.3bits/sec/Hz および 1.6bits/sec/Hz の高い伝送容量が得られることを明らかにしている．

キーワード　RF 適応アレーアンテナ，MIMO 伝送，伝送容量，アンテナ選択，エスパアンテナ，ビームステアリング，アンテナ評価

Performance Evaluation of RF Adaptive Array Antennas Based on Indoor Propagation Measurement

Hiroya TANAKA†, Kriangsak SIVASONDHIVAT†, Jun-ichi TAKADA†, Atsushi HONDA††,
Sorwar HOSSAIN††, Ichirou IDA††, and Yasuyuki OISHI††

† Tokyo Institute of Technology　2–12–1–S6–4, O-okayama, Meguro-ku, Tokyo 152–8550
†† Fujitsu Ltd.　5–5, Hikari-no-Oka, Yokosuka-shi, Kanagawa 239–0847
E-mail: †{tanaka,joe,takada}@ap.ide.titech.ac.jp
††{ahonda@labs.fujitsu.com, s.hossain@jp.fujitsu.com, ida.ichirou@jp.fujitsu.com, yasu@labs.fujitsu.com}

Abstract　Performance improvement by adaptive array antennas (AAA) that can be controlled in the radio frequency (RF) process (RF-AAA) has been reported in MIMO transmissions. For example, (1) antenna selection type AAA by using RF-switches and (2) beam steering type AAA by using variable reactance devices are well-known. Although these RF-AAAs work with different mechanisms, they contribute quite similar benefits to the improvement of the transmission performance. This report focuses on the performance evaluation between these two kinds of RF-AAAs in a 2×2 MIMO transmission scheme by using the measured propagation data in line-of-sight (LOS) and non-LOS (NLOS) environments. As a result, it is revealed that beam steering by ESPAR antenna can provide higher capacity than the antenna selection by RF-switch by 1.3bits/sec/Hz and 1.6bits/sec/Hz in the LOS and NLOS environment, respectively.

Key words　RF adaptive array antenna, MIMO transmission, Capacity, Antenna selection, ESPAR antenna, Beam steering, Antenna evaluation.

1. Introduction

Some adaptive array antennas which can be controlled by using RF components such as switches and variable reactance devices have been reported [1], [2]. This report represents these kind of antennas as RF adaptive array antennas (RF-AAA). The antenna selection by switch is a well-known RF-AAA [1]. By using the switch, the best element is chosen and the transmission performance is improved. On the other hand, an RF-AAA realized by variable capacitors known as the electronically steerable parasitic array radiator (ESPAR) antenna can also be used [2]. The ESPAR antenna has an excited element and some parasitic elements which are loaded

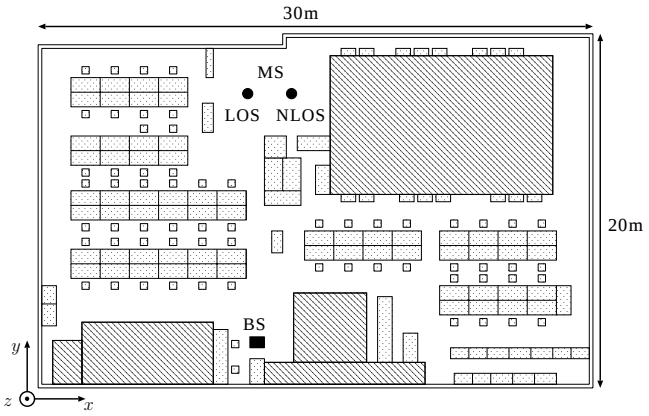

Fig. 1 Measurement environment

with a variable capacitor. By controlling the bias voltages applied to the variable capacitors, beam steering is achieved.

Although these RF-AAAs have different working mechanisms, we obtain a similar benefit that is the improvement of transmission performance by changing the antenna characteristics such as the radiation pattern and spatial correlation. However, it is unclear which RF-AAA is more useful, therefore this report focuses on the performance comparison of the RF-AAAs realizing antenna selection by the switch (RF-AAA-AS) and beam steering by ESPAR antennas (RF-AAA-BS) in a 2×2 MIMO transmission scheme. The system employs the patch antennas for the elements. The evaluation is performed from the viewpoint of transmission capacity by using the propagation data measured in an office environment.

2. Measurement Description and Results

The propagation models extracted from the measured data are used in order to evaluate the RF-AAAs. This section addresses the measurement system, environment and results.

2. 1 Measurement System and Environment

The Medav RUSK Fujitsu sounder is used in the measurement [3]. The test signal is a periodic multitone signal with a center frequency of 4.5GHz and bandwidth of 120MHz. The base station (BS) antenna is a 2 × 4 uniform rectangular antenna array of dual polarized patch antenna elements. At the mobile station (MS) side, a 2-ring circular antenna array is used. One ring is composed of 24 dual-polarized patch antenna elements.

The measurement was carried out in an indoor office environment. The map is shown in Fig. 1. The slash and dot parts imply small rooms divided by metallic partition walls and objects such as desk, chair, rack and so on, respectively. The BS and MS antennas were placed on a tripod stand and cart, respectively. The measurement was performed in line-of-sight (LOS) and non-LOS (NLOS) environment.

2. 2 Measurement Results

Multidimensional gradient based maximum-likelihood estimator is used to extract the channel parameters from the measurement data [4]. Each path is modeled jointly by angle of departure (AOD) and arrival (AOA), time delay, and polarimetric complex path weights. Figures 2 and 3 show the power angular distributions of detected paths in LOS and NLOS environment, respectively. The path weights are normalized by the total power of reconstructed paths. The AOA of VV- and HV-component and delay are shown in Fig. 2 and 3. Note that VV and HV indicate co- and cross-polarization components of vertical transmissions. Legends in these figures imply the power ratio of each path. Figure 4 illustrates the delay distribution of detected paths. Extracted power ratios from the total received signals are 78% and 19% in LOS and NLOS, respectively. Moreover, mean XPRs are 4.8dB and 5.3dB, respectively. Almost all paths are coming from around azimuth -90° and 130° in LOS and NLOS environment, respectively.

3. Analysis Method and Evaluation Criteria

The analysis method and evaluation criterion are discussed herewith. Note that this report treats only the downlink side so that "Tx" and "Rx" is used to describe the BS and MS, respectively. Moreover, vertical polarized omni directional antennas are used at Tx in the simulation.

3. 1 Analysis Method

In wideband MIMO systems where the number of Tx and Rx antennas are L_{Tx} and L_{Rx}, the relation between received signal vector $\boldsymbol{y}(t) \in C^{L_{\mathrm{Rx}}}$ and transmitted signal vector $\boldsymbol{s}(t) \in C^{L_{\mathrm{Tx}}}$ are expressed as

$$\boldsymbol{y}(t) = \int \boldsymbol{H}(\tau)\boldsymbol{s}(t-\tau)\mathrm{d}\tau + \boldsymbol{n}(t), \tag{1}$$

$$\tilde{\boldsymbol{y}}(f) = \tilde{\boldsymbol{H}}(f)\tilde{\boldsymbol{s}}(f) + \tilde{\boldsymbol{n}}(f) \tag{2}$$

where $\boldsymbol{H}(\tau) \in C^{L_{\mathrm{Rx}} \times L_{\mathrm{Tx}}}$ and $\boldsymbol{n}(t) \in C^{L_{\mathrm{Rx}}}$ are the MIMO channel matrix and noise vector, respectively. And also, $\tilde{\boldsymbol{y}}$, $\tilde{\boldsymbol{H}}$, $\tilde{\boldsymbol{s}}$, and $\tilde{\boldsymbol{n}}$ are Fourier transformations of $\boldsymbol{y}$, $\boldsymbol{H}$, $\boldsymbol{s}$, and $\boldsymbol{n}$. Note that Eqs. (1) and (2) assume that the channel is quasi-static. Hereafter, τ and f are discretized, and then m and k imply indices of discretized delay time $\tau = m\Delta\tau$ and frequency $f = k\Delta f$, respectively. Hence, discretized channel matrix $\boldsymbol{H}(m)$ and $\tilde{\boldsymbol{H}}(k)$ are used in the subsequent discussions.

The elements of $\boldsymbol{H}$ are described by superposition of all paths from the transmitting antenna l_{Tx} ($l_{\mathrm{Tx}} = 1, \cdots, L_{\mathrm{Tx}}$) to the receiving antenna l_{Rx} ($l_{\mathrm{Rx}} = 1, \cdots, L_{\mathrm{Rx}}$) as shown below.

$$[\boldsymbol{H}]_{l_{\mathrm{Rx}} l_{\mathrm{Tx}}} = \sum_u h_{u,l_{\mathrm{Rx}} l_{\mathrm{Tx}}}, \tag{3}$$

$$\begin{aligned} h_{u,l_{\mathrm{Rx}} l_{\mathrm{Tx}}} &= h_{\mathrm{V}u,l_{\mathrm{Rx}} l_{\mathrm{Tx}}} E_{\mathrm{V},l_{\mathrm{Rx}}}(\theta_u, \phi_u) \\ &\quad + h_{\mathrm{H}u,l_{\mathrm{Rx}} l_{\mathrm{Tx}}} E_{\mathrm{H},l_{\mathrm{Rx}}}(\theta_u, \phi_u), \end{aligned} \tag{4}$$

$$h_{\mathrm{V}u,l_{\mathrm{Rx}} l_{\mathrm{Tx}}} = \eta_{\mathrm{V},u} \exp(j\varphi_{u,l_{\mathrm{Tx}}})\, a_{u,l_{\mathrm{Rx}}}, \tag{5}$$

$$h_{\mathrm{H}u,l_{\mathrm{Rx}} l_{\mathrm{Tx}}} = \eta_{\mathrm{H},u} \exp(j\varphi_{u,l_{\mathrm{Tx}}})\, a_{u,l_{\mathrm{Rx}}}, \tag{6}$$

$$a_{u,l_{\mathrm{Rx}}} = \exp\left(j\frac{2\pi d_{l_{\mathrm{Rx}}}}{\lambda}\cos(\frac{\pi}{2} - \phi_u)\sin(\theta_u)\right), \tag{7}$$

where subscript $[\boldsymbol{H}]_{ij}$, E_{V} and E_{H} imply the (i,j) entry of matrix $\boldsymbol{H}$, vertical and horizontal component of complex E-field gain E. Note that $\boldsymbol{H}$ and E are changed by the adaptation. u is an index number for the path. In addition, η_u

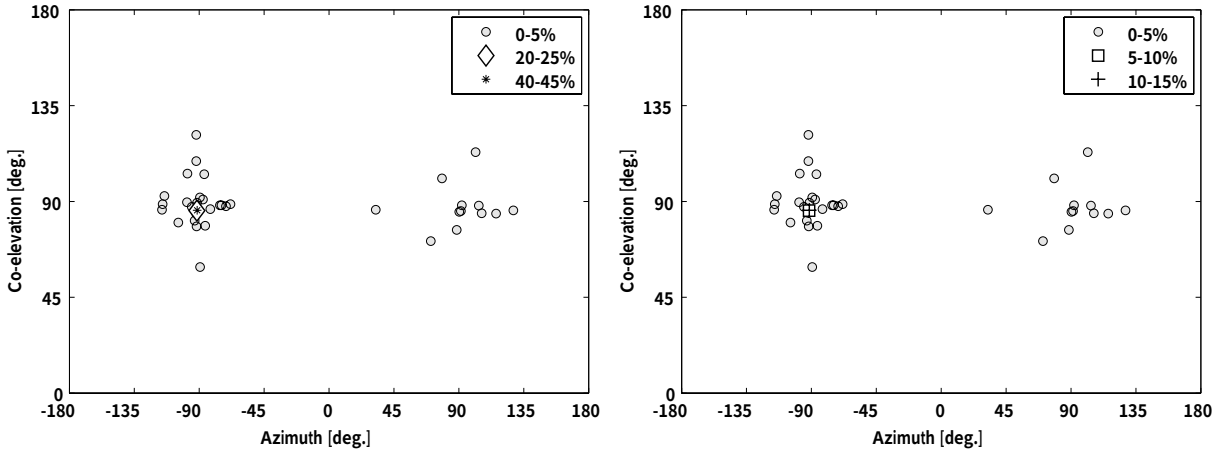

(a) Angular distribution (VV)

(b) Angular distribution (HV)

Fig. 2 Angular power distribution of detected paths at MS (LOS)

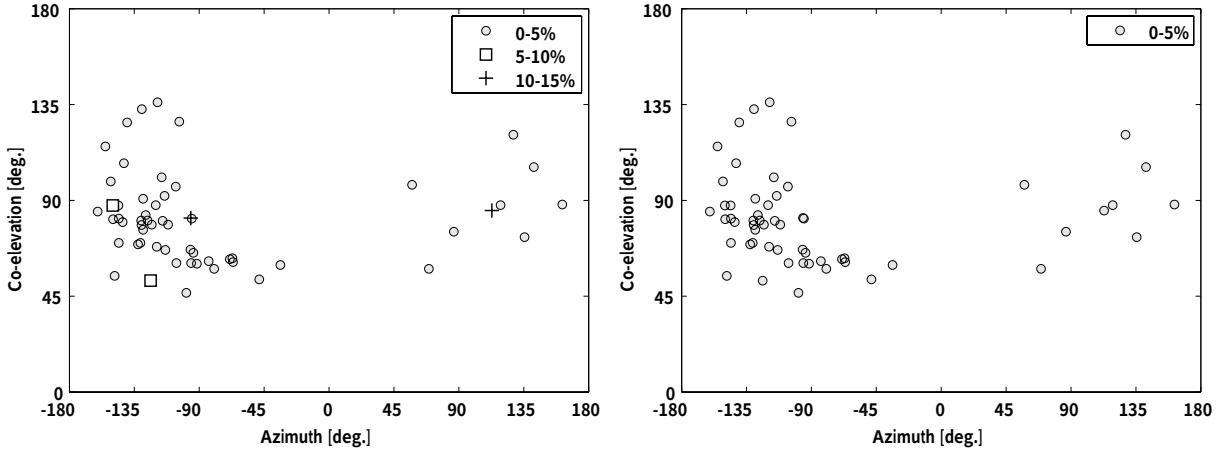

(a) Angular distribution (VV)

(b) Angular distribution (VV)

Fig. 3 Angular power distribution of detected paths at MS (NLOS)

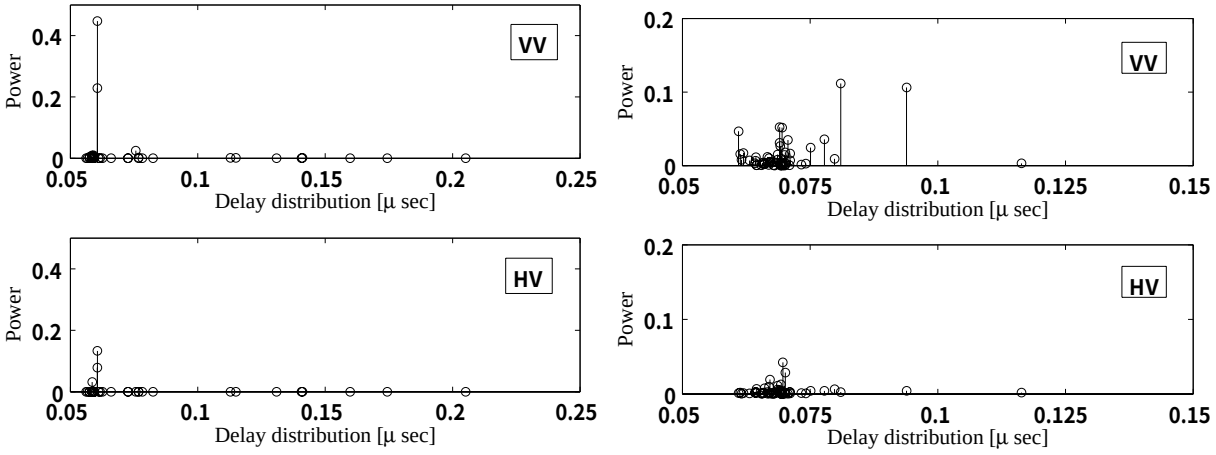

(a) Delay distribution (LOS)

(b) Delay distribution (NLOS)

Fig. 4 Power delay distribution of detected paths

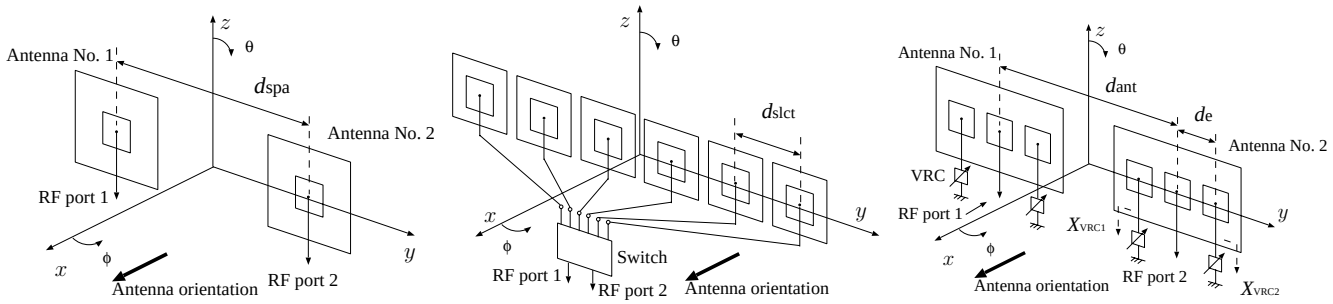

(a) single elements (SE) (b) RF-AAA-AS (c) RF-AAA-BS

Fig. 5 Considered configuration of antennas

and $\varphi_{u,l_{\mathrm{Tx}}}$ are the amplitude and phase component of the path weight with respect to u and l_{Tx}. Array factor $a_{u,l_{\mathrm{Rx}}}$ is expressed by $d_{l_{\mathrm{Rx}}}$, ϕ_u and θ_u, which are the distance from coordinate origin to antenna and azimuth and coelevation angles component of AOA, respectively.

$\varphi_{u,l_{\mathrm{Tx}}}$ are randomly generated from a uniform distribution over $[0, 2\pi)$ in every snapshot according to the random phase method. Note that discretized ϕ_u and θ_u rounded by 1° step are used in the simulation. Delay is also rounded by sampling timing 0.05μsec. In addition, only the extracted paths are used to reconstruct incoming waves. This means that the diffused component is not considered in the discussion.

3. 2 Evaluation Criteria

This report adopts the transmission capacity as the criterion to evaluate the antenna performance. Utilizing Eqs. (1) to (7), the instantaneous channel capacity $c(k)$ for a subcarrier can be calculated in case of space division multiplexing like below.

$$c(k) = \log_2 \det \left(\tilde{\boldsymbol{H}}(k) \tilde{\boldsymbol{H}}^H(k) \frac{P}{\sigma^2} + \boldsymbol{I}_{N_{\mathrm{Rx}}} \right) \tag{8}$$

where $\boldsymbol{I}_{N_{\mathrm{Rx}}} \in C^{N_{\mathrm{Rx}}}$, P and σ^2 are the identity matrix, transmitting power of single element and noise power.

4. Antenna configurations and characteristics

Effectivenesses of a 2×2 MIMO transmission is compared when configurations below are used in the receiver.

(a) Single elements (SE)
(b) RF-AAA-AS
(c) RF-AAA-BS

Figure 5 illustrates the layout of SE, RF-AAA-AS and RF-AAA-BS. Both RF-AAAs consist of six patch antennas and two RF ports. A linear array within 6λ is considered to simplify discussions. The RF-AAA-AS can be realized by the switch. It selects two elements from all candidates. While the RF-AAA-BS is configured with two ESPAR antennas composed of three elements. The parasitic elements are loaded with variable reactance circuits (VRC). By changing the input impedances of the VRCs, beam steering is realized.

4. 1 Radiation Pattern

Figures 6 and 7 show examples of radiation patterns given by each RF-AAA. The antenna orientation is 0° in Figs. 6 and 7. These results are calculated by HFSS and infinite ground plane is assumed. Figure 6 shows the amplitude of E-field gain of a patch antenna. Note that we ignore the mutual coupling between each element in the RF-AAA-AS so that every element in the RF-AAA-AS shall have identical radiation patterns as Fig. 6.

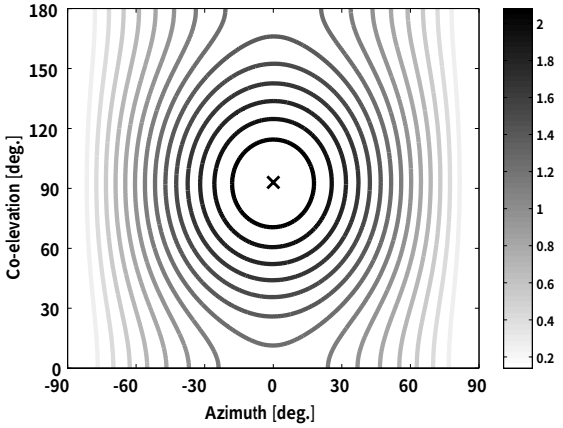

Fig. 6 E-field of vertical polarization (patch antenna)(× implies the peak.)

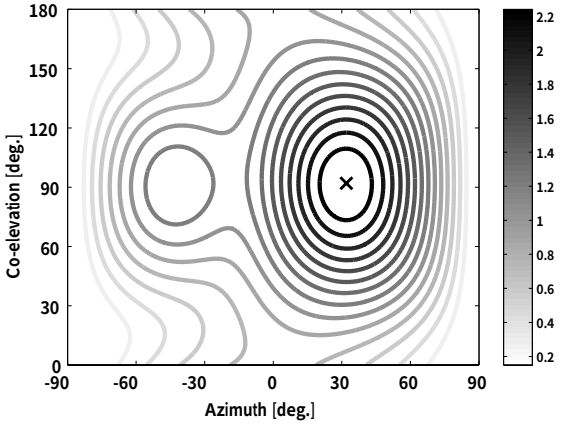

Fig. 7 E-field of vertical polarization (ESPAR antenna $(X_{\mathrm{VRC1}}, X_{\mathrm{VRC2}}) = (1.5, -2.0)$)(× implies the peak.)

The distances between excited and parasitic elements are set as $d_{\mathrm{e}} = 0.4\lambda$ in the ESPAR antenna. This value is determined to be well-suited from the aspect of impedance match-

ing and beam steerable range. Figure 7 indicates an example of the amplitude of E-field gain where the input reactances of VRCs are $(X_{\mathrm{VRC1}}, X_{\mathrm{VRC2}}) = (1.5, -2.0)$. Note that X_{VRC} is normalized by the impedance of the transmission line. The peak radiated direction is 30° in Fig. 7. The variable range of X_{VRC} is applied from -2.0 to 1.5 [2] so that it is obvious that the maximum beam steerable range is ±30°.

4. 2 Adjustment of RF-AAAs

In RF-AAA-AS, the antenna combination giving the best capacity is selected for an instantaneous channel. In RF-AAA-BS, X_{VRC} has a continuous quantity so that it is impossible to calculate 'all' realizations of radiation patterns for 'all' reactance values. Therefore, we use the radiation patterns by the X_{VRC} discretized by five values, which are $X_{\mathrm{VRC}} = 1.5$, 0.625, -0.25, -1.125 and -2.0. And then, the resulting radiation patterns are treated as candidates for selection. The combination giving the best capacity is selected from them.

4. 3 Design of Element Layout

The elements of SE and each RF-AAA shall be allocated within 6λ along the y-axis. They are designed so as to work effectively in the measured propagation environment. First, the design concept of SE is discussed here. Generally speaking, low spatial correlation results in high transmission capacity and therefore correlation coefficient can be a useful criterion in order to determine the effective layout. Correlation coefficient $\tilde{\rho}_{ij,pq}$ between channels ij and pq is expressed as

$$\tilde{\rho}_{ij,pq} = \frac{1}{K}\sum_{k} \frac{\left\langle \left[\tilde{\boldsymbol{H}}(k)\right]^{*}_{ij} \left[\tilde{\boldsymbol{H}}(k)\right]_{pq} \right\rangle}{\sqrt{\left\langle \left| \left[\tilde{\boldsymbol{H}}(k)\right]_{ij} \right|^2 \right\rangle} \sqrt{\left\langle \left| \left[\tilde{\boldsymbol{H}}(k)\right]_{pq} \right|^2 \right\rangle}}, \tag{9}$$

where notation $\langle \cdot \rangle$ is defined as the average for the total number of sampling. Figure 8 shows $\tilde{\rho}_{11,21}$ in case when the distance between elements are varied in SE whose antenna orientation is $-90°$. It is obvious that $d_{\mathrm{spa}} = 6.0\lambda$ and $d_{\mathrm{spa}} = 1.0\lambda$ provide lower correlation in the LOS and NLOS environment, respectively.

Secondly, the layout of RF-AAA-AS is determined. RF-AAA-AS shall be a uniform linear array to simplify the discussion. Therefore, the layout of elements are designed so as to satisfy the lower correlation between nearest elements, that is d_{slct} is set as 1.0λ in each environment.

Finally, the layout of RF-AAA-BS is discussed. Figure 8 also show $\tilde{\rho}_{11,21}$ of the ESPAR antennas. In order to calculate $\tilde{\rho}_{11,21}$ for an instantaneous channel realization, we use the conditions of X_{VRC} giving the maximum capacity under the adjustment method in section 4. 2. According to Fig. 8 as well as the SE and RF-AAA-AS, the distances between center antennas are set as $d_{\mathrm{ant}} = 5.0\lambda$ and $d_{\mathrm{ant}} = 4.5\lambda$ in the LOS and NLOS environment, respectively. The element layouts are summarized in Table 1.

5. Simulation Results and Discussions

The analysis is dedicated to wireless LAN so that the simulation is based on the IEEE 802.11a communication system.

Table 1 Antenna layout

	d_{spa}	d_{slct}	d_{ant}	d_{e}
LOS	1.0λ	1.0λ	5.0λ	0.4λ
NLOS	6.0λ	1.0λ	4.5λ	0.4λ

Table 2 Simulation Condition

Center frequency	4.5GHz
Number of transmitting antennas L_{Tx}	2
Number of receiving antennas L_{Rx}	2
Number of snapshots	10,000
Number of subcarriers K	48
Bandwidth	20MHz
Received SNR in case when vertical polarized omni directional antennas are used in BS	10dB

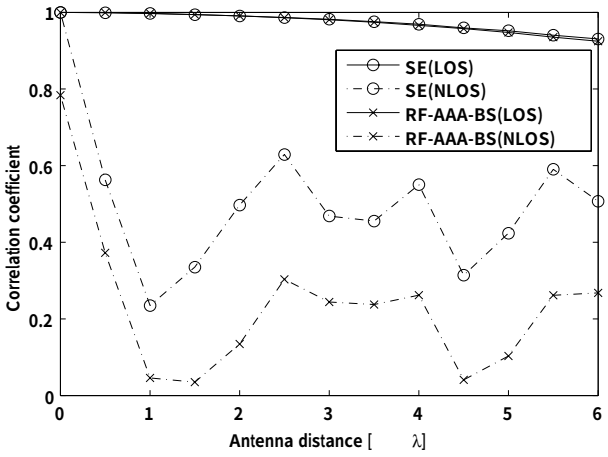

Fig. 8 Correlation coefficient $\tilde{\rho}_{11,21}$

The simulation condition is written in Table 2. Transmitted power is normalized to satisfy that received power becomes 10dB in both environments when vertical polarized omni directional antennas are used in Rx side.

Figure 9(a) shows the average received SNR at port 1 and $\tilde{\rho}_{11,21}$ in case when the antenna orientations are changed from $-170°$ to $-10°$ in the LOS environment. Moreover, Fig. 9(b) illustrates average capacity $\langle c \rangle$. It is obvious that the RF-AAA-BS is better than the SE and RF-AAA-SA in the LOS environment. Figure 10 shows simulated results in the NLOS environment similar to Fig. 9. In this case, Both RF-AAA-BS and RF-AAA-AS can provide higher capacity than SE.

Two factors can cause the improvement of capacity. The first one is a decrease of correlation brought by the adaptive controls. Lower correlation can increase the received SNR and also realize high independence between channels. The second factor is an increase of received SNR due to the beam steering. This effect is found only in the ESPAR antenna. In the LOS environment, the correlation is quite high so that the antenna selection is not working effectively. However, the capacity improvement is achieved just only in RF-AAA-BS due to the increase of received SNR by the beam steering. In the NLOS environment, both RF-AAAs are working well when the antenna orientations are from $-150°$ to $-90°$. In both environments, degradation occurs due to the mismatch between the AOA of almost all paths and peak radiated direction of antenna. Even then RF-AAA-BS enhances the

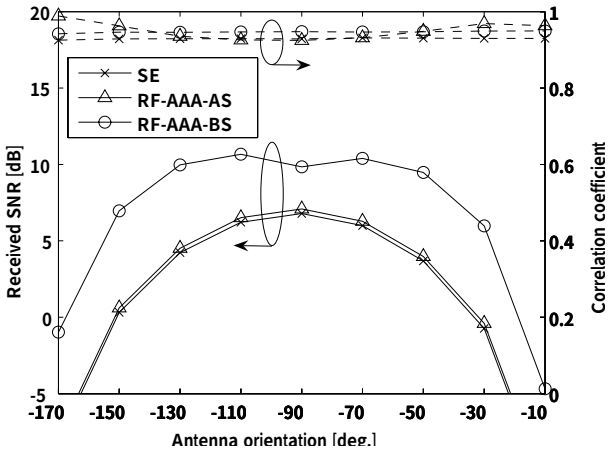

(a) Received SNR of Port 1 and correlation coefficient.

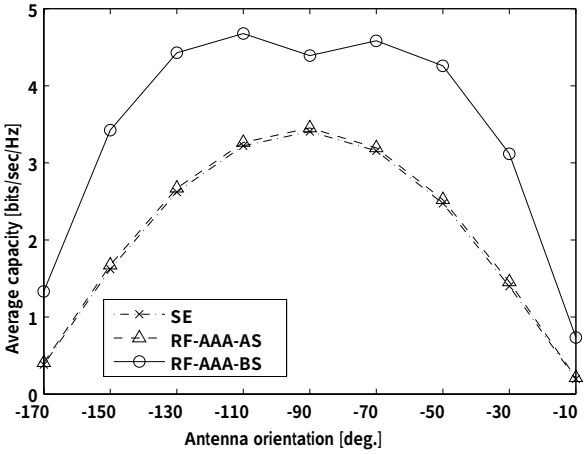

(b) Average capacity.

Fig. 9 Transmission characteristics when the antenna orientations are changed in the LOS environment.

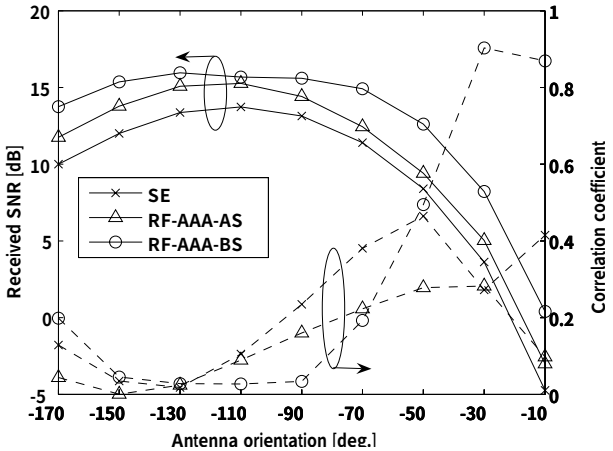

(a) Received SNR of Port 1 and correlation coefficient.

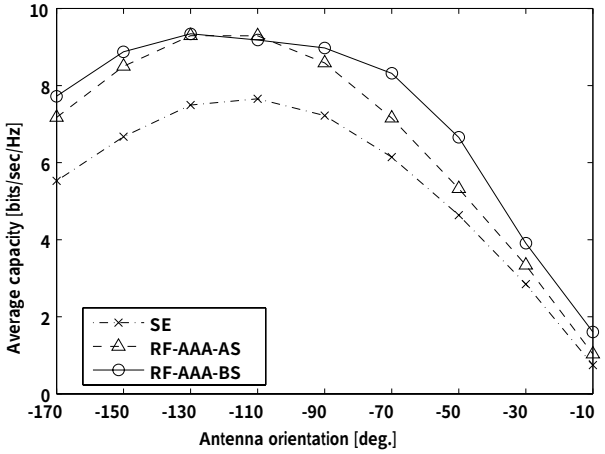

(b) Average capacity.

Fig. 10 Transmission characteristics when the antenna orientations are changed in the NLOS environment.

Table 3 Averaged capacity

	SE	RF-AAA-AS	RF-AAA-BS
LOS	2.1	2.1	3.4
NLOS	5.4	5.6	7.2

(unit : bits/sec/Hz)

capacity through beam steering. Table 3 shows the capacities averaged over all orientation. We can see that the RF-AAA-BS realizes higher capacities than the RF-AAA-AS by 1.3bits/sec/Hz and 1.6bits/sec/Hz in the LOS and NLOS environment, respectively.

Acknowledgment

This research is supported by the National Institute of Information and Communications Technology of Japan.

References

[1] A. F. Molisch et al., "MIMO systems with antenna selection," IEEE Microwave Magazine, vol.5, pp.46–56, Mar. 2004.

[2] H. Tanaka, J. Takada, A. Honda, I. Ida, Y. Oishi, "Capacity Analysis by Planar ESPAR Antenna in MIMO Transmission," IEEE Resion 10 Conference (TENCON2006), SS1.4, Nov. 2006.

[3] http://www.channelsounder.de.

[4] R. S. Thoma, M. Landmann, and A. Richter, "RIMAXA Maximum Likelihood Framework for Parameter Estimation in Multidimensional Channel Sounding," 2004 Intl. Symp. on Antennas and Propagation (ISAP 2004), pp.53–56, Japan, Aug. 2004.

[5] K. Sakaguchi, and J. Takada, "Measurement, Analysis, and Modeling of MIMO Propagation Channel," IEICE Trans. B, vol.J88-B, no.9, pp.1624-1640, Sept. 2005. (in Japanese)